

# Adsorption of CH<sub>3</sub>S and CF<sub>3</sub>S on Pt(111) surface: a density functional theory study

Y. Cardona Quintero · H. Zhu · R. Ramprasad

Received: 10 August 2012 / Accepted: 1 November 2012 / Published online: 27 November 2012  
© Springer Science+Business Media New York 2012

**Abstract** Density functional theory calculations have been performed to study binding modes of adsorbed CX<sub>3</sub>S (X = H and F) on Pt(111) for a large range of adsorbate coverages and the consequent work function shifts. We find that these properties are all strongly correlated to the surface coverage. Depending on the molecular coverage on Pt surface, the work function shift may be as large as 0.7 eV for Pt–CH<sub>3</sub>S and 1.5 eV for Pt–CF<sub>3</sub>S with respect to the clean surface value. Two factors contribute to the work function shift: the charge transfer between the molecule and the surface, and the molecular dipole moment. While the charge transfer contribution always tend to decrease the work function, the molecular dipole moment contribution for the CH<sub>3</sub>S and CF<sub>3</sub>S cases are oppositely directed. Thus, appropriate choices of molecular components and control of surface coverage would be effective techniques to tune the work function of the metal surfaces.

## Introduction

Self-assembled monolayers (SAMs) of organic molecules have found wide applications in catalysis, surface protection, and organic electronics [1–4] enabled, in part, by the tunability of various surface properties through the

adequate choice and conformation of the SAMs [5]. In the field of organic electronics, SAMs interfaced with a metal electrode have been utilized as one critical component of nano-devices [6]. The performances of these devices strongly depend on the chemical bonding at the metal–organic interface and the work function of the system.

These technological drivers have spurred extensive efforts devoted to careful studies of adsorption of SAMs on several different metal surfaces (i.e., Au, Ni, Pt, Pd, Ag, and Cu) both theoretically and experimentally [7–17]. Although a variety of SAMs have been studied, methyl thiolate (CH<sub>3</sub>S) and trifluoromethyl-thiolate (CF<sub>3</sub>S) have been studied the most due to the good anchoring properties of these thiolate groups and their simple structures [5, 9, 10]. It is, by now, well accepted that the metal–SAM properties such as the favored geometry, the adsorption energy, and the work function may be controlled in many ways. For instance, the molecular coverage of CH<sub>3</sub>S on metal surfaces controls both the favored geometry and the adsorption energy [10]. Additionally, the variation of the components of the CX<sub>3</sub>S molecule (X = H or F) can control the work function of the metal–CX<sub>3</sub>S system. Previous experimental and computational studies in metals such as Au and Ag showed that the adsorption of CH<sub>3</sub>S decreased the work function of the metal–CH<sub>3</sub>S system with respect to that of the clean metal, while the adsorption of CF<sub>3</sub>S on the same metals increased the work function of the system [5]. These findings were rationalized initially in terms of the dipole moment of the molecules [18], but later on, were understood as a consequence of the dipole moment at the metal–SAM interface [14, 19]. Another important conclusion that emerges from prior studies is that the work function shifts do not depend strongly upon the CX<sub>3</sub>S surface coverage for the Au–CX<sub>3</sub>S and Ag–CX<sub>3</sub>S systems (X = H or F). This behavior was explained by comparing

Y. Cardona Quintero · H. Zhu · R. Ramprasad (✉)  
Department of Chemical, Materials and Biomolecular  
Engineering, Institute of Materials Science, University of  
Connecticut, 97 North Eagleville Road, Storrs, CT 06269, USA  
e-mail: rampi@uconn.edu

Y. Cardona Quintero  
e-mail: yenny.cardona\_quintero@uconn.edu

two phenomena occurring with the increase in the molecular coverage: an increase in the work function shift due to increasing density of molecular dipoles, and a decrease in the work function shift due to increasing depolarizing fields. According to previous studies, these two factors tend to cancel one another in those systems making the work function shift independent of the molecular coverage [14, 19].

Much less is known pertaining to the Pt–CX<sub>3</sub>S system at various CX<sub>3</sub>S surface coverages. Experimentally, the adsorption of CH<sub>3</sub>S on Pt was observed at temperatures close to 223 K with the formation of an ordered ( $\sqrt{3} \times \sqrt{3}$ )R30° LEED pattern [20, 21]. Previous computational studies have addressed the geometry and adsorption energy of Pt–CX<sub>3</sub>S for limited surface coverages and limited or constrained geometries [9, 10]. Prior DFT work for the ( $\sqrt{3} \times \sqrt{3}$ )R30° coverage [5] also showed that the work function of the Pt–CX<sub>3</sub>S system decreased with respect to that of the clean Pt, for both molecules. This behavior contrasts with that displayed by Au–CX<sub>3</sub>S and Ag–CX<sub>3</sub>S. It indicates that the dipole created from the bonding between the thiolate molecules and the metal surfaces strongly depends upon the metal [5].

This contribution attempts to critically assess the behavior of Pt–CX<sub>3</sub>S systems, using the first principles density functional theory (DFT). As the most stable surface for Pt, the (111) surface is considered and the adsorption of CH<sub>3</sub>S and CF<sub>3</sub>S corresponding to various surface coverages is explored comprehensively. Five molecular coverages of the Pt(111) surface (c.f., Fig. 1a) and two adsorption sites on the Pt(111) surface, namely the fcc and hcp positions (c.f., Fig. 1b), are considered in this study. We find that the geometry, adsorption energy, and the work function shifts of the Pt–CX<sub>3</sub>S systems vary with the surface coverage (rather than the adsorption site, i.e., fcc or hcp). An important outcome that emerges from this investigation is that while the work function of both the Pt–CH<sub>3</sub>S and Pt–CF<sub>3</sub>S systems is always smaller than that of the clean Pt surface (for all surface coverages considered), the work function shift displayed by the Pt–CH<sub>3</sub>S system is much smaller than that of the Pt–CF<sub>3</sub>S system. This interesting behavior is explained in terms of the molecular dipole moment and charge transfer contributions to the overall work function shifts.

This paper is organized as follows. In “Computational details” section, we provide details pertaining to the computational method and models adopted. Our results for the geometry of the gas phase molecules and the Pt–CX<sub>3</sub>S systems are presented in “Geometry” section. The “Absorption energy” section contains a discussion of the molecular adsorption energies and their dependence on surface coverage. The “Work function” section covers a

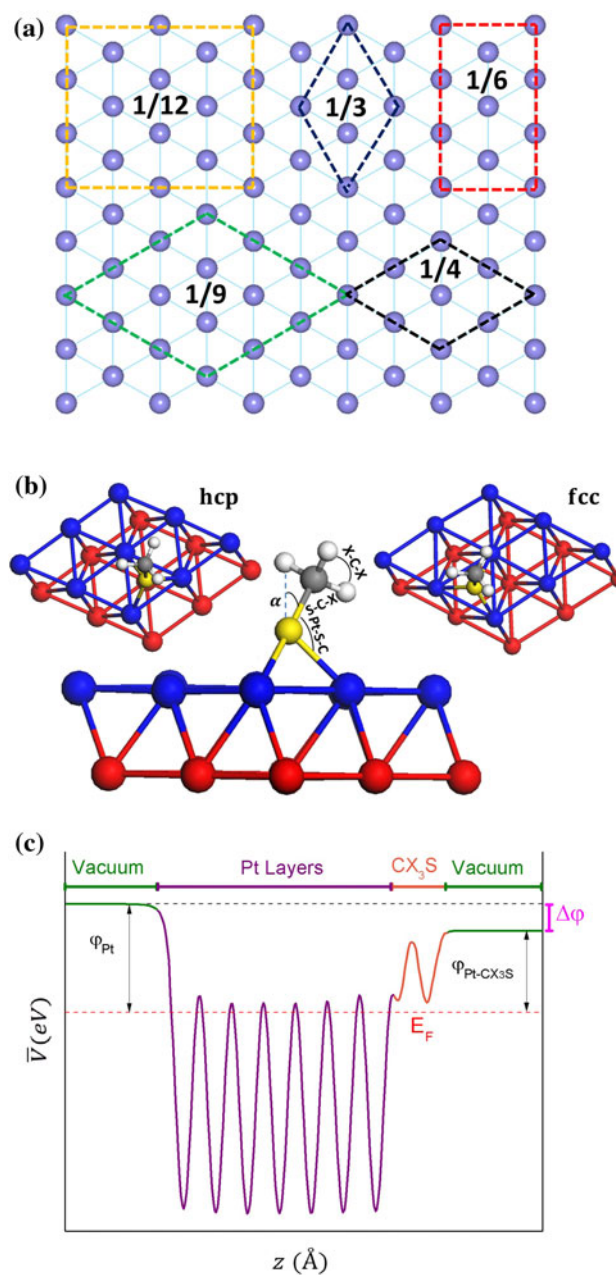


**Fig. 1** **a** Surface unit cells adopted for different adsorption coverages ( $\theta = 1/3, 1/4, 1/6, 1/9,$  and  $1/12$ , corresponding, respectively, to ( $\sqrt{3} \times \sqrt{3}$ )R30°, ( $2 \times 2$ ), ( $\sqrt{3} \times 3$ ), ( $3 \times 3$ ), and ( $2\sqrt{3} \times 3$ )) considered in this study. **b** hcp and fcc positions of the molecule on the Pt(111) surface and geometric parameters of the Pt–CX<sub>3</sub>S system. **c** Planar average potential of the Pt–CX<sub>3</sub>S system along the surface normal direction. The potentials for each part (vacuum, Pt slab, and CX<sub>3</sub>S molecules) are indicated in the figure. The red dashed line stands for the Fermi energy of Pt. Vacuum on left side with respect to  $E_F$  is the work function for clean surface ( $\phi_{Pt}$ ), while the vacuum level on right side with respect to  $E_F$  is the work function of the Pt–CX<sub>3</sub>S system ( $\phi_{Pt-CX_3S}$ ) (Color figure online)

critical assessment of the work function shift as a function of coverage. The “Summary” section is devoted to the summary and conclusions of our work.

### Computational details

The DFT calculations were performed using the Vienna ab initio simulation package (VASP) code [22], using the Perdew–Burke–Ernzerhof (PBE) generalized gradient approximation (GGA), the projector-augmented wave approach, and a cutoff energy of 400 eV for the plane wave expansion of the wave functions. van der Waals interactions have also been taken into account using the Grimme DFT-D2 functional [23]. The calculated results were converged such that the atomic forces were smaller than 0.02 eV/Å

The Pt(111) surface was studied using a slab supercell containing seven Pt layers and a 12–15 vacuum region. Three layers in the center were fixed at their bulk positions and the remaining layers close to the surfaces were allowed to relax. The most stable structures of the molecules, CX<sub>3</sub>S with X = H or F, were obtained by relaxing from several different initial geometries as reported in the literature [9, 10, 24]. Five molecular coverages  $\theta = 1/3, 1/4, 1/6, 1/9,$  and  $1/12$  monolayer (ML) (corresponding to  $(\sqrt{3} \times \sqrt{3})R30^\circ, (2 \times 2), (\sqrt{3} \times 3), (3 \times 3),$  and  $(2\sqrt{3} \times 3)$ , respectively) and two adsorption sites (fcc and hcp) were considered, as shown in Fig. 1a, b, respectively.

To investigate the properties of CX<sub>3</sub>S on the Pt surface, we adopted an asymmetric slab supercell with just the top surface of the slab covered by the CX<sub>3</sub>S molecules. Dipole corrections were used to account for the artificial field on the system caused by the repeating supercells. The work function is computed by matching the planar average local electrostatic potential of the surface system and that of the corresponding Pt bulk system, and computing the difference between the vacuum level (of the surface system) and the Fermi energy (of the bulk system) as schematically shown in Fig. 1c [25]. The planar average potential in the vacuum part of the side with the molecule (right side of

Fig. 1c) was used to calculate the work function of the Pt–CX<sub>3</sub>S system ( $\phi_{\text{Pt-CX}_3}$ ), while the planar average potential on the clean surface side (left side in Fig. 1c) provides the work function of the clean Pt surface ( $\phi_{\text{Pt}}$ ). Using this method, we determined the work function shift ( $\Delta\phi$ ) as  $\phi_{\text{Pt-CX}_3\text{S}} - \phi_{\text{Pt}}$  (See “Work function” section)

### Geometry

CH<sub>3</sub>S and CF<sub>3</sub>S in the gas phase

The geometry of gas phase CH<sub>3</sub>S and CF<sub>3</sub>S is summarized in Table 1. The predicted structural parameters of CH<sub>3</sub>S are close to previously reported theoretical values [9, 26], and in good agreement with experimental values [24, 27] with a maximum bond length and bond angle discrepancy of 0.023 Å and 4.16°, respectively. For CF<sub>3</sub>S, the maximum differences of bond lengths and the bond angles between this work and experiments [28] are 0.039 Å and 1.59°, respectively. From Table 1, we note that the S–C bond for CH<sub>3</sub>S and CF<sub>3</sub>S are equal; however, the C–H bond is shorter than the C–F bond. The predicted S–C–F angles are larger than the S–C–H ones, and the X–C–X angles, for both X = H and F, are close to the tetrahedral angle (109.5°). We also note that the geometrical parameters in the isolated molecules with and without van der Waals interactions (DFT and DFT-D2) are very close, indicating that intra-molecular van der Waals interactions are not significant here.

Geometry of the Pt–CX<sub>3</sub>S system

The Pt–CX<sub>3</sub>S system was built by placing one isolated CX<sub>3</sub>S on the Pt(111) surface for five coverages ( $\theta = 1/3, 1/4, 1/6, 1/9,$  and  $1/12$ ) and two positions (fcc and hcp).

**Table 1** Predicted bond lengths and bond angles of the isolated CX<sub>3</sub>S (X = H, F) molecules, along with other experimental and theoretical results

	CH <sub>3</sub> S				CF <sub>3</sub> S			
	This work PBE	This work DFT-D2	Other DFT [9]	Expt. [24]	This work PBE	This work DFT-D2	Other DFT [29]	Expt. [28]
Bond length (Å)								
S–C	1.8	1.8	1.8	1.8	1.8	1.8	1.8	1.8
C–X1	1.1	1.1	1.1	1.1	1.4	1.4	1.3	1.3
C–X2, C–X3	1.1	1.1	1.1	1.1	1.4	1.4		
Bond angle (°)								
S–C–X1	107.5	107.3	106.4	111.5	108.9	108.9		
S–C–X2, S–C–X3	111.6	111.7	112.1	111.5	112.4	112.6	110.8	
X1–C–X2	106.1	106.0	107.4		106.8	106.7		
X1–C–X, X2–C–X3	109.9	109.9	111.2		108.0	107.9		109.5

The geometrical parameters obtained with the PBE and DFT-D2 functionals, such as bond lengths, bond angles, tilt angles ( $\alpha$ ), and favored adsorption position after relaxation, are reported in Tables 2 and 3, respectively, for the Pt-CH<sub>3</sub>S and Pt-CF<sub>3</sub>S systems.

Our results indicate that the difference in the bond angles and bond lengths of Pt-CX<sub>3</sub>S between PBE and DFT-D2 levels of theory are in the ranges of  $\pm 2^\circ$  and  $\pm 0.02$  Å, respectively. The difference in the geometry of the CH<sub>3</sub>S molecule before and after its adsorption on the Pt(111) surface (Tables 1, 2, 3) is minor. Also, the final geometries of Pt-CH<sub>3</sub>S and Pt-CF<sub>3</sub>S, in general, are very similar although the S-C and C-X bonds of the latter are slightly longer than those of the former. Considering the

similarity between Pt-CH<sub>3</sub>S and Pt-CF<sub>3</sub>S, we briefly discuss the results for the former below.

The tilt angle for Pt-CH<sub>3</sub>S has been reported before [9, 10], but discrepancies exist between different studies. Ghiringhelli et al. [10] found rather small tilt angles of  $1.4^\circ$  and  $0.6^\circ$  for the fcc and hcp positions for the Pt-CH<sub>3</sub>S system in a 1/3 ML molecular coverage with an initial vertical configuration of molecules. Karhanek et al. [9] studied both the vertical and tilted configurations. They reported final tilt angles of  $0^\circ$  for fcc and hcp positions with a vertical initial configuration and  $34.8^\circ$  and  $36.5^\circ$  for these two adsorption sites when an initial tilted configuration is adopted. The latter study also reported that the tilted configuration is more stable than the vertical configuration,

**Table 2** Predicted tilt angle, bond angles, and bond lengths for the Pt-CH<sub>3</sub>S system (as defined in Fig. 1b) at the PBE level of theory

Coverage	Position	Pt-CH <sub>3</sub> S							Site after relaxation
		Tilt angle ( $^\circ$ )	Bond angle ( $^\circ$ )			Bond length (Å)			
		$\alpha$	Pt-S-C	S-C-H	H-C-H	Pt-S	S-C	C-H	
1/3	fcc	40.8 (44.7)	115	108	111	2.31	1.85	1.10	fcc-bridge
	hcp	47.6 (47.6)	116	109	110	2.31	1.83	1.10	hcp-bridge
1/4	fcc	19.8 (19.9)	116	108	111	2.26	1.85	1.10	fcc
	hcp	22.1(23.5)	116	108	111	2.28	1.85	1.10	hcp
1/6	fcc	18.4 (18.5)	120	108	111	2.26	1.85	1.09	fcc
	hcp	20.5 (20.6)	138	107	111	2.31	1.84	1.10	hcp
1/9	fcc	17.8 (17.6)	129	108	111	2.28	1.85	1.10	fcc
	hcp	19.7 (19.8)	116	107	112	2.27	1.83	1.10	hcp
1/12	fcc	14.5 (14.4)	121	107	112	2.25	1.83	1.10	fcc
	hcp	19.0 (17.7)	114	107	112	2.27	1.84	1.10	hcp

The results in parenthesis correspond to DFT-D2 results. The DFT-D2 results for the bond angles were in the range of  $\pm 2^\circ$ , and the bond lengths were in the range of  $\pm 0.02$  Å with respect to the PBE values and hence are not shown here

**Table 3** Predicted tilt angle, bond angles, and bond lengths for the Pt-CF<sub>3</sub>S system (as defined in Fig. 1b) at the PBE level of theory

Coverage	Position	Pt-CF <sub>3</sub> S							Site after relaxation
		Tilt angle ( $^\circ$ )	Bond angle ( $^\circ$ )			Bond length (Å)			
		$\alpha$	Pt-S-C	S-C-F	F-C-F	Pt-S	S-C	C-F	
1/3	fcc	34.4 (41.1)	115	110	109	2.31	1.92	1.35	fcc-bridge
	hcp	32.4 (32.5)	121	110	109	2.30	1.90	1.36	hcp
1/4	fcc	22.0 (22.0)	114	110	109	2.29	1.95	1.35	fcc
	hcp	32.3 (33.0)	113	110	109	2.31	1.92	1.35	hcp
1/6	fcc	20.2 (20.2)	118	110	109	2.28	1.92	1.35	fcc
	hcp	24.2 (24.2)	111	110	109	2.31	1.95	1.35	hcp
1/9	fcc	19.9 (19.9)	114	110	109	2.28	1.94	1.34	fcc
	hcp	26.4 (26.5)	113	110	109	2.31	1.93	1.35	hcp
1/12	fcc	19.0 (18.7)	119	110	109	2.27	1.93	1.35	fcc
	hcp	20.4 (20.2)	111	109	110	2.28	1.90	1.34	hcp

The results in parenthesis correspond to DFT-D2 results. The DFT-D2 results for the bond angles were in the range of  $\pm 2^\circ$ , and the bond lengths were in the range of  $\pm 0.02$  Å with respect to the PBE values and hence are not shown here

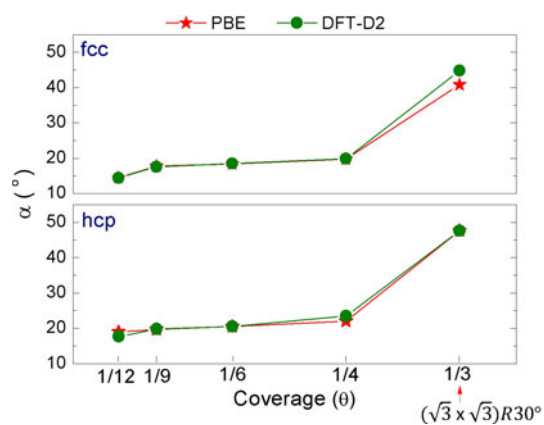


**Fig. 2** Tilt angle of Pt–CH<sub>3</sub>S system as a function of molecular coverage ( $\theta$ ) calculated using PBE and DFT-D2 functionals

such as the one reported by Ghiringhelli et al. [10] corresponding to a local minimum [9]. For the Pt–CF<sub>3</sub>S system, no geometric information has been reported previously.

The tilt angle for Pt–CH<sub>3</sub>S in both fcc and hcp adsorption sites, for the two levels of theory considered here (PBE and DFT-D2) is shown in Fig. 2 and reported in Tables 2 and 3. The largest tilt angle for the Pt–CH<sub>3</sub>S system was found at  $\theta = 1/3$  for both fcc and hcp sites with values of 40.8° and 47.6°. For the other coverages, the values of the tilt angles are all close and increase slightly with molecular coverage, probably due to the larger interaction between the molecules. The tilt angle, according to the results presented here is the parameter that changes the most with the variation of the coverage.

In general, the bond lengths and bond angles are very similar for the different coverages, in agreement with prior work [10]. Additionally, there is a difference in the adsorption site of the molecule before and after relaxation for  $\theta = 1/3$ . A slight movement from the fcc and hcp to fcc-bridge and hcp-bridge sites was observed, also consistent with previous work [9].

### Adsorption energy

The adsorption energy per CX<sub>3</sub>S molecule on the Pt surface is given by

$$E_{\text{ads}} = E_{\text{Pt-CX}_3\text{S}} - E_{\text{Pt}} - E_{\text{CX}_3\text{S}}, \quad (1)$$

where  $E_{\text{Pt-CX}_3\text{S}}$ ,  $E_{\text{Pt}}$  and  $E_{\text{CX}_3\text{S}}$  are the energies of the Pt–CX<sub>3</sub>S system, the clean Pt surface, and the gas phase CX<sub>3</sub>S molecule, respectively. The obtained adsorption energies of the Pt–CF<sub>3</sub>S and Pt–CH<sub>3</sub>S systems for the adsorption coverage and adsorption sites considered are shown in Fig. 3. Several interesting observations may be made. First, we note that the adsorption energy for the fcc site is almost always lower than that for the hcp site (and thus more

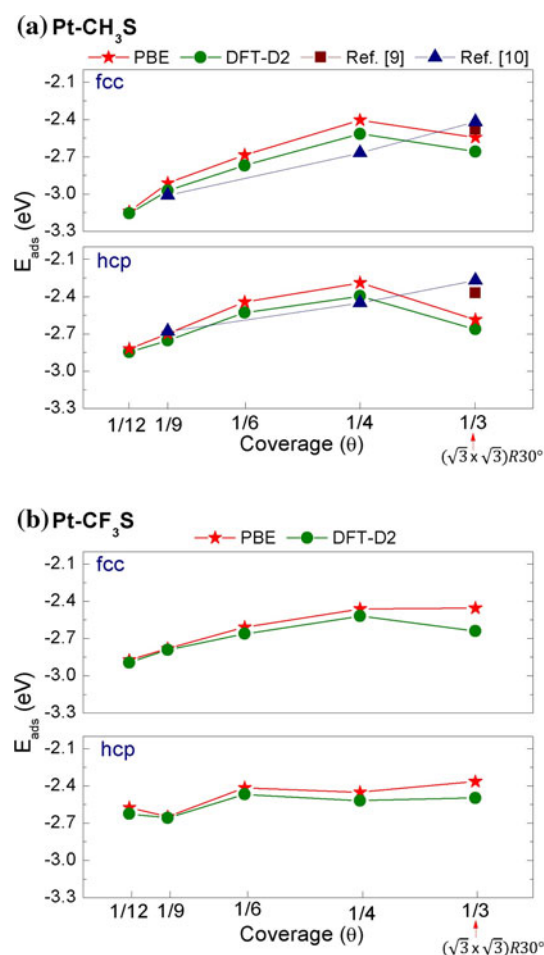


**Fig. 3** Adsorption energies ( $E_{\text{ads}}$ ) of **a** CH<sub>3</sub>S and **b** CF<sub>3</sub>S molecules on Pt surfaces in different coverage and adsorption sites

favorable) for all the systems considered, with the exception of the  $\theta = 1/3$  case for CH<sub>3</sub>S. However, as mentioned before, the final position for this coverage changes to an fcc-bridge site after relaxation.

Second, depending on the coverage,  $E_{\text{ads}}$  ranges from about –2.4 to –3.1 eV for the fcc site and from about –2.3 to –2.8 eV for the hcp site for both Pt–CH<sub>3</sub>S and Pt–CF<sub>3</sub>S systems. The lowest  $E_{\text{ads}}$  for the fcc site is obtained at the coverage of  $\theta = 1/12$  for both CH<sub>3</sub>S and CF<sub>3</sub>S. This coverage corresponds to the most dilute adsorption situation considered in this study. In general,  $E_{\text{ads}}$  decreases monotonically with coverage up to  $\theta = 1/4$  with the exception of CF<sub>3</sub>S at the hcp site. However,  $E_{\text{ads}}$  decreases with the further increase of  $\theta$  from 1/4 to 1/3, indicating that the high coverages may be particularly stabilized. This result is consistent with experiments which indicate the preferential adsorption of CH<sub>3</sub>S on Pt for  $\theta = 1/3$  ML (corresponding to  $(\sqrt{3} \times \sqrt{3})R30^\circ$  LEED pattern). An interesting factor that accompanies the increased stability at this coverage is the difference in the geometry at  $\theta = 1/3$  with respect to that at the other coverages. The tilt angle at  $\theta = 1/3$

much larger (c.f., Fig. 2) and the molecule at this coverage also experiences a change of position after relaxation from the hollow to the hollow-bridge position. We also note from Fig. 3 that in all cases the DFT-D2 values are lower than the PBE values. As the coverage increases, the differences between the two methods become more obvious due to the stronger intermolecular interaction at higher coverages.

Figure 3 also provides a comparison of the present results with available previous results pertaining to the adsorption energies of  $\text{CH}_3\text{S}$  molecules at the fcc and hcp sites. Ghiringhelli et al. [10] report  $E_{\text{ads}}$  for  $\text{CH}_3\text{S}$  on Pt with  $\theta = 1/3$ ,  $1/4$ , and  $1/9$  (Fig. 3a) with a vertical molecule as the final adsorption configuration. The results obtained by Karhanek et al. [9] (also shown in Fig. 3), as well as our own work, suggest that geometries with negligible or zero tilt angles are local minima or saddle points.

### Work function

The adsorption of  $\text{CX}_3\text{S}$  on the Pt surface causes a change of the surface dipole moment and hence, in a work function shift ( $\Delta\phi$ ), as defined earlier (c.f., Fig. 1c)

$$\Delta\phi = \phi_{\text{Pt-CX}_3\text{S}} - \phi_{\text{Pt}} \quad (2)$$

Molecules such as  $\text{CH}_3\text{S}$  and  $\text{CF}_3\text{S}$  display oppositely directed dipole moments. When these molecules are adsorbed on metals such as Au and Ag,  $\Delta\phi$  also displays opposite sign. However, in the case of Pt, it was found that  $\Delta\phi$  is negative with respect to the clean metal for both  $\text{CH}_3\text{S}$  and  $\text{CF}_3\text{S}$  [5]. This implies that there is an additional factor that contributes to  $\Delta\phi$  which will be clarified below.

The total  $\Delta\phi$  of the  $\text{Pt-CX}_3\text{S}$  system may be partitioned into two main contributions, namely the molecular dipole moment contribution ( $\Delta\mu$ ) and the bonding or charge transfer contribution ( $\Delta\nu$ ), as follows:

$$\Delta\phi = \Delta\mu + \Delta\nu, \quad (3)$$

$$\Delta\mu = \frac{eD}{\epsilon_0 A} \quad (4)$$

where  $D$  represents the molecular dipole moment,  $\epsilon_0$  is the permittivity of vacuum,  $e$  is the charge of an electron, and  $A$  is the surface area of Pt containing a single molecule.  $D$  was obtained from the calculations of each isolated molecule fixed at the geometry corresponding to the adsorbed states. Using Eq. 4, one can obtain  $\Delta\mu$ . With the values of  $\Delta\phi$  and  $\Delta\mu$  and using Eq. 3,  $\Delta\nu$  may then be determined.

Figure 4 shows  $\Delta\phi$ ,  $\Delta\mu$  and  $\Delta\nu$  for the  $\text{Pt-CH}_3\text{S}$  (Fig. 4a) and  $\text{Pt-CF}_3\text{S}$  (Fig. 4b) systems for the fcc adsorption position as a function of coverage. Owing to the very different electronegativities of H and F, the dipole

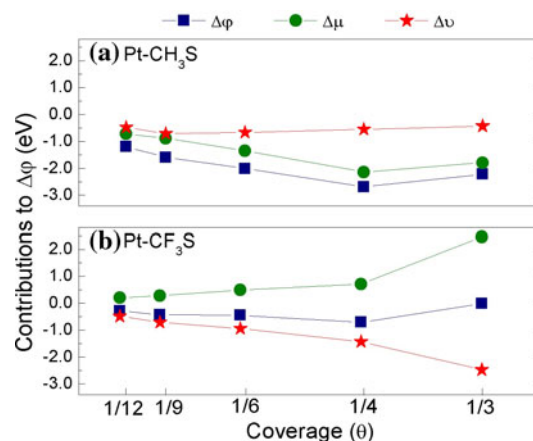


**Fig. 4** Work function variation ( $\Delta\phi$ ), molecular dipole moment contribution ( $\Delta\mu$ ), and charge transfer contribution ( $\Delta\nu$ ) for the **a**  $\text{Pt-CH}_3\text{S}$  and **b**  $\text{Pt-CF}_3\text{S}$  systems in the fcc position as a function of molecular coverage ( $\theta$ )

moments of  $\text{CH}_3$  and  $\text{CF}_3$  are indeed oppositely directed, and consequently,  $\Delta\mu$  displays opposite signs in the two cases.  $\Delta\nu$ , on the other hand, displays the same sign in the two classes of systems (albeit much larger in  $\text{Pt-CF}_3\text{S}$ ). Thus, in the case of  $\text{Pt-CF}_3\text{S}$ ,  $\Delta\nu$  and  $\Delta\mu$  tend to cancel each other and makes  $\Delta\phi$  close to zero. However, because  $\Delta\nu$  and  $\Delta\mu$  are both negative for  $\text{Pt-CH}_3\text{S}$ , the magnitude of  $\Delta\phi$  is much larger in this case. By separating the work function changes into charge transfer and molecular dipole moment contributions, we conclude that the different behaviors of  $\text{CX}_3\text{S}$  on Pt and Ag are likely caused by the very different charge transfer in the two cases. Indeed, this conclusion is supported by the very different work functions of the clean Pt and Ag metal surfaces ( $\phi_{\text{Pt}} = 5.65$  eV,  $\phi_{\text{Ag}} = 4.26$  eV). In the  $\text{Ag-CF}_3\text{S}$  system, the charge transfer is directed from the metal to the molecule as alluded to before [5], unlike in the  $\text{Pt-CF}_3\text{S}$  system.

Our results have a good agreement with prior theoretical works. Rusu and Brocks calculated  $\Delta\phi$  of the  $\text{Pt-CH}_3\text{S}$  and  $\text{Pt-CF}_3\text{S}$  systems for  $\theta = 1/3$  to be  $-2.39$  and  $-0.16$  eV, respectively, which agrees well with our predictions ( $-2.22$  and  $-0.01$  eV) [5]. The remaining discrepancies between this study and prior results can be attributed to the different levels of theory and the possible differences in geometry between the systems (Rusu and Brocks did not report the geometry of their systems).

Most interestingly, we note from Fig. 4 that the work function of  $\text{Pt-CX}_3\text{S}$  is strongly dependent on the adsorption coverage. The highest (0.01 eV) and the lowest ( $-0.71$  eV)  $\Delta\phi$  for  $\text{CF}_3\text{S}$  were obtained for  $\theta = 1/3$  and  $1/4$  ML, respectively. For  $\text{CH}_3\text{S}$ , the highest and the lowest  $\Delta\phi$  were obtained for  $\theta = 1/4$  ( $-1.20$  eV) and for  $\theta = 1/9$  ( $-2.70$  eV), respectively, with a large tunability of 1.5 eV. Thus, controlling the molecular concentration on the Pt surface may be a useful technique to tune the work

function. This behavior is very different from the prior observation for Au–CX<sub>3</sub>S and Ag–CX<sub>3</sub>S, in which the work function shift has a relatively weak dependence on the packing density (i.e., the molecular coverage) [14, 19].

## Summary

The geometry, adsorption energy, and work function of CH<sub>3</sub>S and CF<sub>3</sub>S on the Pt(111) surface at various coverages have been investigated in this study. Our results can be summarized as follows:

1. In both the Pt–CH<sub>3</sub>S and Pt–CF<sub>3</sub>S systems, the tilt angle, adsorption energy, and work function shifts are coverage dependent.
2. The adsorption energy of the Pt–CH<sub>3</sub>S and Pt–CF<sub>3</sub>S systems was almost always lower in the fcc site than in the hcp one.
3. van der Waals interactions between adsorbed molecules do not have an important effect in the systems studied here.
4. A special preference for the  $\theta = 1/3$  coverage in the case of the Pt–CH<sub>3</sub>S system is seen. This is consistent with the experimentally observed  $(\sqrt{3} \times \sqrt{3})R30^\circ$  LEED pattern.
5. The work function variation is controlled by two components: the molecular dipole moment contribution and the charge transfer contribution. The former displays opposite signs for Pt–CH<sub>3</sub>S and Pt–CF<sub>3</sub>S systems, while the latter has the same sign.
6. The work function of both Pt–CH<sub>3</sub>S and Pt–CF<sub>3</sub>S systems is smaller than that of the clean Pt surface. Depending on the molecular coverage on the Pt surface, the work function can be varied by a large degree (0.7 eV for Pt–CH<sub>3</sub>S and 1.5 eV for Pt–CF<sub>3</sub>S). Control of molecular coverage on the Pt surface, and proper choice of the molecule, could be an effective technique to tune the metal surface work function.

**Acknowledgements** Financial support of this study through a Grant from the National Science Foundation (NSF) and computational support through a NSF Teragrid Resource Allocation are gratefully acknowledged. Helpful discussions with Prof. Ramanath (RPI) are also gratefully acknowledged.

## References

1. Schreiber F (2000) *Prog Surf Sci* 65:151
2. Grill L (2008) *J Phys Condens Matter* 20:053001
3. Li Z, Chang S, Williams RS (2003) *Langmuir* 19:6744
4. Stammer X, Tonigold K, Bashir A, Kfer D, Shekhah O, Hlsbusch C, Kind M, Gross A, Wll C (2010) *Phys Chem Chem Phys* 12:6445
5. Rusu PC, Brocks G (2006) *Phys Rev B* 74:073414
6. Kucera J, Gross A (2008) *Langmuir* 24:13985
7. Rusu PC, Giovannetti G, Weijtens C, Coehoorn R, Brocks G (2009) *J Phys Chem C* 113:9974
8. Maksymovych P, Sorescu DC, Yates JT Jr (2006) *J Phys Chem B* 110:21161
9. Karhanek D, Bucko T, Hafner J (2010) *J Phys Condens Matter* 22:265005
10. Ghiringhelli LM, Caputo R, Site LD (2007) *J Phys Condens Matter* 19:176004
11. Ohara M, Kim Y, Kawai M (2006) *Jpn J Appl Phys* 45:2022
12. Lee S, Park J, Ragan R, Kim S, Lee Z, Lim DK, Ohlberg DAA, Williams RS (2006) *J Am Chem Soc* 128:5745
13. Jiao J, Bu SY, Wang GC, Bu XH (2008) *J Mol Struct (Theochem)* 862:80
14. Rusu PC, Giovannetti G, Brocks G (2007) *J Phys Chem C* 111:14448
15. Boer B, Hadipour A, Mandoc MM, Woudenbergh T, Blom PWM (2005) *Adv Mater* 17:621
16. Campbell H, Rubin S, Zawodzinski TA, Kress JD, Martin RL, Smith DL (1996) *Phys Rev B* 54:14321
17. Zehner RW, Parsons BF, Hsung RP, Sita LR (1999) *Langmuir* 15:1121
18. Alloway DM, Hofmann H, Smith DL, Gruhn NE, Graham AL, Colorado R Jr, Wysocki VH, Lee TR, Lee PA, Armstrong NR (2003) *J Phys Chem B* 107:11690
19. Rusu PC, Brocks G (2006) *J Phys Chem B* 110:22628
20. Lee JJ, Fisher CJ, Bittencourt C, Woodruff DP, Chan ASY, Jones RG (2002) *Surf Sci* 516:1
21. Kim SS, Kim Y, Kim HI, Lee TR, Perry SS, Rabalais JW (1998) *J Chem Phys* 109:9574
22. Kresse G, Furthmuller J (1996) *Phys Rev B* 54:11169
23. Grimme S (2006) *J Comp Chem* 27:1787
24. Hsu YC, Liu X, Miller TA (1989) *J Chem Phys* 90:6852
25. Zhu H, M. Aindow M, Ramprasad R (2009) *Phys Rev B* 80:201406; Zhu H, Ramprasad R (2011) *J Appl Phys* 109:083719
26. El Bouzaidi RD, El Hammadi A, Boutalib A, El Mouhtadi M (2000) *J Mol Struct (Theochem)* 497:197
27. Lide DR (2001) *CRC handbook of chemistry and physics*, 81st edn. CRC Press LLC, Boca Raton
28. Yang MC, Williamson JM, Miller TA (1997) *J Mol Spectrosc* 186:1
29. Marenich AV, Boggs JE (2006) *Int J Quantum Chem* 106:2609